

Article

# Joint Message-Passing and Convex Optimization Framework for Energy-Efficient Surveillance UAV Scheduling

Soyi Jung <sup>1</sup>, Joongheon Kim <sup>2</sup>  and Jae-Hyun Kim <sup>1,\*</sup> 

<sup>1</sup> Department of Electrical and Computer Engineering, Ajou University, Suwon 16499, Korea; sogloomy@ajou.ac.kr

<sup>2</sup> School of Electrical Engineering, Korea University, Seoul 02841, Korea; joongheon@korea.ac.kr

\* Correspondences: jkim@ajou.ac.kr; Tel.: +82-31-219-2474

Received: 5 August 2020; Accepted: 8 September 2020; Published: 9 September 2020



**Abstract:** In modern surveillance systems, the use of unmanned aerial vehicles (UAVs) has been actively discussed in order to extend target monitoring areas, even for an extreme circumstances. This paper proposes an energy-efficient UAV-based surveillance system that operates from two different sequential methods. First, the proposed algorithm pursues energy-efficient operations by deactivating selected surveillance cameras on the UAVs located in overlapping areas. For this objective, a message-passing based algorithm is used because the overlapping situations can be formulated using a max-weight independent set. Next, the unscheduled UAVs based on the message-passing fly to the charging towers to be charged. This algorithm computes the optimal matching between the UAVs and charging towers and the amount of energy allocation for the scheduled UAV-tower pairs. This joint optimization is initially formulated as non-convex, and it is then reformulated to be convex, which can guarantee optimal solutions. The proposed framework achieves the desired performance, as presented in the performance evaluation.

**Keywords:** UAVs; surveillance; energy efficiency; charging scheduling; optimization

## 1. Introduction

The deployment of mobile autonomous surveillance systems has received considerable attention by academic and industrial societies for smart city security applications. In particular, the use of unmanned aerial vehicles (UAVs) allows surveillance, even in extreme conditions [1,2].

However, the deployment of UAVs for surveillance applications is associated with serious research challenges, and one of the major challenges is that UAV-based systems are extremely power hungry. In modern UAV systems, the commercial UAV battery lifetime is extremely short, (e.g., dozens of minutes), whereas the charging time is at least two times longer. Therefore, energy-efficient operations are required for reliable UAV-based surveillance system operations by increasing the operating hours of UAVs. In this paper, we characterize a charging infrastructure that is composed of wireless ground-mounted charging towers. The charging towers can acquire unlimited power from ground and wirelessly charge the UAVs through their charging panels. For the energy-efficient UAV-based surveillance system operations, two sequential methods are proposed in this paper, i.e., (i) micro in-device energy-efficient operation and (ii) macro system wide energy-efficient operation.

For micro in-device energy-efficient operation, a new method can reduce energy consumption in UAV-based surveillance systems by turning off select closed-circuit television (CCTV) cameras on the UAVs monitoring overlapping areas. To algorithmically formulate this, an overlapping model that is based on a max-weight independent set (MWIS) is used in this paper. By solving this MWIS-based

formula, a set of UAVs can be selected and scheduled, and their CCTV cameras can be activated for surveillance. Here, we have to note that the MWIS problem is a well-known NP-hard problem [3]. Many approaches exist in order to solve the problem and, among them, a solution approach that is based on message-passing is investigated in this paper, which was inspired by the literature on wireless interference modeling [3].

For macro systemwide energy-efficient operation, we design a new charging mechanism for energy-limited UAV systems. Based on wireless energy transfer technologies [4–8], the UAVs that need to be charged can fly to charging towers for obtaining energy resources over a wireless medium. Based on this setting, we propose a new optimal control mechanism for charging matching between UAVs and charging towers. In addition, this mechanism determines the amount of energy allocation for the matched UAV-tower pairs. This joint optimization of matching and resource/energy allocation is a non-convex optimization framework, which cannot guarantee optimal solutions in polynomial time. To resolve this problem, we reformulate the mathematical optimization program into a convex programming framework that is equivalent to the original non-convex formulation. Finally, the reformulated convex programming framework can compute the optimal solutions in polynomial time.

Based on these two sequential methods, we confirm that our proposed UAV-based surveillance system is able to conduct energy-efficient operations through (i) the minimization of overlapping surveillance areas with message-passing to solve the MWIS formulation and then (ii) the convex optimization of the matching decision between UAVs and charging towers and the associated energy allocation decision for the matched UAV-tower pairs. Throughout the data-intensive performance evaluation with various settings, we confirm that our proposed algorithm with these two sequential methods outperform the others.

The main contributions of this paper can be summarized, as follows.

- This research is the first attempt to characterize the overlapping surveillance areas with MWIS formulation that is feasible in practice. In the MWIS-based model, we design a novel solution approach that is based on the concept of message-passing.
- We determine that the optimization problem for joint matching and energy allocation between UAVs and charging towers is non-convex. We then present a novel method for transforming the non-convex formulation into the convex programming, thus achieving optimal solutions.
- In addition to the theoretical novelties, we conduct data-intensive simulations with various simulation settings. It is demonstrated that our joint matching and energy allocation method remarkably outperforms several baseline schemes. Furthermore, our proposed matching and energy allocation algorithm between UAVs and charging towers presents the desired performance improvement.

The rest of this paper is organized as follows. Section 2 summarizes the related work for UAV communications and networks research. Section 3 introduces our considered reference system model. Section 4 explains the details of the proposed algorithm, (i.e., (i) MWIS-based UAV scheduling via message-passing and (ii) joint optimization for charging matching and wireless energy transfer). Section 5 verifies the novelty of the proposed framework via data-intensive performance evaluations. Lastly, Section 6 concludes this paper and presents future research directions.

## 2. Related Work

In literature, there have been many studies on UAV in all aspects of communications and networks research [9–11].

*Radio Propagation and Channel Models.* The radio-wave, propagation, and antenna-related research results in UAV flying networks are well presented in [12]. The detailed summary of wireless channel and radio propagation models in UAV communication networks is given in [13] and, especially, air-to-ground UAV channel models are presented in [14]. For more details, non-stationary

air-to-air UAV wireless channel models are introduced [15]. In addition, three-dimensional (3-D) geometry-based stochastic models for UAV multi-input-multi-output wideband non-stationary are discussed in [16]. Moreover, the usage and corresponding channel models for millimeter-wave wireless technologies [17–20] in UAV wireless networks under the consideration of hovering fluctuations is well-discussed in [21]. Lastly, the statistical channel modeling and radio-wave propagation of free-space optical communication (FSO) fronthaul under the consideration of UAV communications is studied in [22].

*Communications.* The use of UAV systems for 5G millimeter-wave wireless networks and cellular networks is well-discussed in [23–26], respectively. For more details, major communication research topics are in multi-antenna techniques [27,28], the use of millimeter-wave networks for high-throughput UAV networks [21,23,29], interworking with satellite networks for coverage extension [30], the use of UAV for device-to-device networks [31,32], and lastly, communication security for multi-UAV networking systems [33,34].

*Networking.* Most of UAV-based networking research topics and their related representative contributions are as follows. First of all, cell-edge user data offloading via UAV systems for non-uniform heterogeneous cellular networks is discussed in [35]. In addition, routing algorithms under the consideration of wireless charging nodes are designed in [36,37]. Moreover, connectivity-aware robust routing and relay deployment algorithms in UAV networks are well-studied in [38]. Lastly, carrier-sensing-multiple-access with collision-avoidance (CSMA/CA)-based enhanced medium access control algorithms for UAV-relay networks are well-discussed in [39].

*Mobility Management and Trajectory Optimization.* One of the major research topics in UAV networks is mobility management and trajectory optimization [40]. Under the consideration of high and unpredictable mobility in UAV, theoretical performance analyses and discussions are presented in [41,42]. In addition, the joint UAV trajectory and flight-time optimization are presented in [43], and the paper also considered FSO communication, which is beneficial in terms of flexible network management. Moreover, energy-aware trajectory optimization with wireless power transfer methods is discussed in [44]. Furthermore, secure trajectory optimization for multi-UAV networks is discussed in [45,46].

*Energy-Efficiency.* The implementation and energy-aware system operations are discussed in [47]. Furthermore, energy efficiency is one of the key research topics in UAV networks due to the extreme UAV battery/energy limitations. To achieve this goal, an energy-efficient operation, especially for the Internet-of-Things (IoT) applications, is discussed in [48]. In terms of the minimization of wireless energy consumption, the proposed method in [49] pursues a sensor network lifetime extension. Under the consideration of a more realistic energy consumption model in UAVs, the proposed method in [50] minimizes the total flight time of the UAV while allowing sensors to successfully upload data. Moreover, considering the energy consumption of both the user and the UAV, the trade-off between the propulsion energy and wireless energy of the served IoT or user was discussed in [51]. Lastly, energy harvesting technologies are also used for the UAV energy-efficient networking, as presented in [52].

*Applications.* Our considering UAV network is beneficial in many applications due to its scalability in terms of mobile deployment. First of all, the use of UAV networks for 5G and beyond 5G network applications is actively discussed nowadays in industry and academia [11,23,25]. In addition, the use of UAV networks for surveillance, security, and rescue tasks, is also to actively under discussion, as presented in [53–57]. Moreover, distributed deep learning and federated learning applications of UAV networks is introduced in [58]. Furthermore, software-related research results in UAV networks and systems are well summarized in [59,60]. Lastly, a mobile charger study in [61] can be related to UAV charging algorithms, including the proposed algorithm in this paper. However, the mobile charger research in sensor networks has several differences from our proposed UAV charging algorithm: (i) mobile chargers are moving in order to charge power-hungry sensor network devices whereas our proposed algorithm lets the UAVs move to be charged by ground-mounted charging towers; and, (ii) mobile chargers are energy-limited, whereas charging towers in this paper are AC-powered

(that is more realistic, because there is no specific description on how the mobile chargers can be charged in [61]).

### 3. System Model

Suppose that a set of UAVs  $\mathcal{S}$  monitors specific target areas (e.g., high-crime areas, festival venues, and so forth) during specific time periods. Let  $s_i$  denote the surveillance UAVs where  $\forall i \in \{1, \dots, |\mathcal{S}|\}$ . Consider that the UAVs are flying at altitude  $h_i$  and have corresponding circular surveillance areas  $a_i$ , defined as  $a_i = r_i^2 \pi$ , where  $r_i$  is the radius of the surveillance area,  $\forall i \in \{1, \dots, |\mathcal{S}|\}$ . The radius is calculated as  $r_i = h_i \cdot \tan(\text{FoV}/2)$ , where  $\text{FoV}$  is the field of view of the built-in UAV camera. In each unit period  $t$ , the surveillance UAV stays in a place or moves to the next position. We assume that the moving UAV flies along a certain path that consists of a sequence of waypoints, (i.e.,  $\mathbf{p}_i = \{p_i[1], p_i[2], \dots, p_i[t]\}$ ,  $\forall i \in \{1, \dots, |\mathcal{S}|\}$ ). Each UAV has its own initial residual battery status, and it can be charged and discharged by charging and discharging processes, respectively. Furthermore, this process can be formulated with a queue, and its backlog evolves, as follows:

$$Q_i(t+1) \triangleq \max\{0, Q_i(t) - \mu_i(t)\} + \lambda_i(t), \forall i \in \{1, \dots, |\mathcal{S}|\}, \quad (1)$$

where  $Q_i(t)$ ,  $\mu_i(t)$ , and  $\lambda_i(t)$  stand for battery energy status (i.e., queue backlog size) at UAV  $s_i$ , the amount of discharging energy at UAV  $s_i$ , and the amount of charging energy at UAV  $s_i$ , respectively,  $\forall i \in \{1, \dots, |\mathcal{S}|\}$ . The charging process is determined by the hardware and system specifications of the charger at each UAV, and the discharging process depends on the operation of each UAV.

In this paper, each UAV has two operational modes in each unit period  $t$ : (i) hovering during surveillance and (ii) round-trip traveling to a charging tower. Each mode has a different amount of energy expenditure to execute the associated tasks during the period  $t$ . For the first action (hovering), the energy expenditure at UAV  $s_i$  is the combination of hovering and communication-related energy, i.e.,

$$E_i^{hc}(t) \triangleq (P_h + P_c)t, \quad (2)$$

where  $P_h$  and  $P_c$  are the power consumption for hovering and communications, respectively. The blade profile is the power required just to turn the rotor blades. The induced power is the power that is required to overcome the induced drag of lift creation, which is an aerodynamic drag force that occurs whenever a moving object redirects the airflow coming toward it. The power consumption for hovering can be as follows [62,63]:

$$P_h \triangleq \underbrace{\frac{\delta}{8} \rho s A \Omega^3 R^3}_{P_o} + (1+k) \underbrace{\frac{W^{3/2}}{\sqrt{2\rho A}}}_{P_i}, \quad (3)$$

where  $P_o$  and  $P_i$  represent the blade profile power and induced power, respectively. The relevant parameters are explained in Table 1. The communication-related energy is usually much lower than the hovering or propulsion energy (e.g., a few watts [64] versus hundreds of watts [65]). In this paper, we assume that the communication-related power is constant. For the second action (round-trip traveling), the UAV moves from one waypoint to another, in a straight line connecting the two waypoints. The total required expenditure of energy for round-trip traveling of a UAV  $s_i$  is as follows:

$$E_i^{tr}(\Delta t_{tr}, v(t)) \triangleq \int_0^{\Delta t_{tr}} P_p(v(t)) dt, \quad (4)$$

where the round-trip UAV traveling time is denoted by  $\Delta t_{tr}$ , and the instantaneous speed of traveling along the paths is denoted by  $v(t)$ . The propulsion power consumption with speed  $v(t)$  can be modeled, as follows:

$$P_p(v(t)) \triangleq \underbrace{P_o \left( 1 + \frac{3v(t)^2}{U_{tip}^2} \right)}_{\text{blade profile}} + \underbrace{P_i \left( \sqrt{1 + \frac{v(t)^4}{4v_o^4} - \frac{v(t)^2}{2v_o^2}} \right)^{1/2}}_{\text{induced}} + \underbrace{\frac{1}{2} d_0 \rho s A v(t)^3}_{\text{parasite}}, \quad (5)$$

where  $P_o$  and  $P_i$  are the constants defined in (3). The propulsion power consumption of the UAV consists of three components, i.e., the blade profile, induced, and parasitic powers. The blade profile and parasitic powers are quadratically and cubically increase with  $v(t)$ , respectively. In contrast, the induced power decreases as  $v(t)$  increases.

**Table 1.** Energy-related notation and setup parameters [66].

Notation	Value
Aircraft weight including battery and propellers, $W$	1375 g
Rotor radius, $R$	0.4 m
Rotor disc area, $A = \pi R^2$	0.503 m <sup>2</sup>
Number of blades, $b$	4
Rotor solidity, $s = \frac{0.0157b}{\pi R}$	0.05
Blade angular velocity, $\Omega$	300 radius/s
Tip speed of the rotor blade, $U_{tip} = \Omega R$	120
Fuselage drag ratio, $d_0 = \frac{0.0151}{sA}$	0.6
Air density, $\rho$	1.225 kg/m <sup>3</sup>
Mean rotor-induced velocity in hovering, $v_0 = \sqrt{\frac{W}{s\rho A}}$	4.03
Profile drag coefficient, $\delta$	0.012
Incremental correction factor to induced power, $k$	0.1

#### 4. Joint Message-Passing and Convex Optimization Framework for UAV Scheduling

This section includes main algorithm design concepts and contributions (refer to Section 4.1), algorithm details (refer to Section 4.2), and lastly, the computational complexity of the proposed algorithm (refer to Section 4.3).

##### 4.1. Design Concepts and Contributions

The proposed energy-efficient UAV-based surveillance system is designed based on the following concepts.

- First, MWIS-based scheduling is conducted to select UAVs whose cameras can be turned off when the corresponding target areas are monitored by other UAVs (i.e., visually overlapping areas). According to this scheduling, the operational energy consumption for the selected UAVs can be reduced and their surveillance lifetime can be extended. In order to solve this MWIS-based scheduling problem, message-passing is used in this paper because it is a well-known solution for this type of combinatorial problem. More details are in Section 4.2.1.
- Furthermore, the unscheduled UAVs are moved to the charging towers to be charged with wireless energy transfer technologies. Subsequently, our proposed optimization framework determines the charging matching of UAVs to charging towers. In addition, each tower determines how much energy should be delivered to the matched UAVs in order to conduct this matching decision in each unit time. This formulation is a mathematically non-convex optimization; however, we converted the corresponding non-convex terms into convex terms (i.e., the polynomial-time operation can be realized for the given joint matching and charging optimization formulation). More details are in Section 4.2.2.

As discussed above, our first problem aims at the minimization of energy consumption by selecting certain amounts of UAVs those cameras can be turned off when the observing target areas are also monitored by other UAVs (visually overlapping areas). Therefore, the objective of this first problem is about to extend surveillance lifetime by saving energies in UAVs. In addition, the second problem is about to conduct joint optimization for charging matching and energy allocation decision between charging towers and UAVs based on the results of the first problem. The objective of this second problem is to maximize the energy charging amounts to the UAVs.

For the given first problem, the UAVs whose cameras are turned off can be charged for extending surveillance lifetime. The charging should be conducted in an efficient way; thus, the second problem, which works based on the result of the first problem, is required for the energy charging amount maximization, which can be beneficial in terms of surveillance lifetime extension, eventually.

#### 4.2. Algorithm Details

As summarized in Section 4.1, our proposed algorithm consists of two sub-algorithms: (1) UAV scheduling with message-passing (refer to Sections 4.2.1 and 4.2.2) joint optimization for charging matching of UAVs to charging towers and the wireless energy transfer between UAVs and charging towers (refer to Section 4.2.2).

##### 4.2.1. MWIS-Based UAV Scheduling via Message-Passing

Consider an undirected graph  $G = (V, E)$ , where  $V$  and  $E$  are the sets of vertices and edges, respectively. Our objective is to select (or schedule) UAVs that can turn off their own built-in surveillance cameras when the corresponding monitoring areas overlap. Thus, we define a visual interference model, where surveillance is considered successful if no neighbor is simultaneously monitoring the same surveillance area. For scheduling, a conflict graph is organized where the set of vertices is connected by an edge if the corresponding vertices cannot be scheduled simultaneously. Based on this concept, the conflict graph can be formulated by an adjacency matrix, whose  $\mathcal{A}_{(i,j)}$  between  $s_i \in \mathcal{S}$  and  $s_j \in \mathcal{S}$  are defined, as follows:

$$\mathcal{A}_{(i,j)} \triangleq \begin{cases} 1, & \text{if } s_i \text{ interferes with } s_j \text{ where } s_i \in \mathcal{S}, s_j \in \mathcal{S}, \text{ and } i \neq j. \\ 0, & \text{otherwise.} \end{cases} \quad (6)$$

The set of neighbors of  $s_i$  is defined, as follows:

$$\mathcal{N}(i) \triangleq \{s_j \mid \mathcal{A}_{(i,j)} = 1, \text{ where } s_j \in \mathcal{S}\}, \forall s_i \in \mathcal{S}. \quad (7)$$

We consider determining the set of vertices of the conflict graph where adjacent connected vertices via the edges cannot be simultaneously selected. This is equivalent to the case that maximizes the summation of weights of all possible independent sets in a given conflict graph. Thus, scheduling can be formulated with MWIS, as follows [3]:

$$\max : \quad \sum_{\forall s_k \in \mathcal{S}} w_k \mathcal{I}_k, \quad (8)$$

$$\text{s.t.} \quad \mathcal{I}_i + \mathcal{I}_j + \mathcal{A}_{(i,j)} \leq 2, \forall s_i \in \mathcal{S}, \forall s_j \in \mathcal{S}, \quad (9)$$

$$\mathcal{I}_i \in \{0, 1\}, \forall s_i \in \mathcal{S}, \quad (10)$$

where

$$\mathcal{I}_i \triangleq \begin{cases} 1, & \text{if } s_i \text{ is scheduled where } s_i \in \mathcal{S}, \\ 0, & \text{otherwise,} \end{cases} \quad (11)$$

where  $w_k$  is a positive integer weight that is associated at each node, and it can be formulated, as follows, in each unit period of time  $t$ :

$$w_k \triangleq Q_k(t), \forall s_k \in \mathcal{S}, \quad (12)$$

where  $Q_k(t)$  stands for the battery energy status of UAV  $s_k$ , as defined in (1).

The above formulation ensures that conflicting UAVs are not scheduled simultaneously. If  $\mathcal{A}_{(i,j)} = 0$  (no edges between  $s_i$  and  $s_j$ ), then  $\mathcal{I}_i + \mathcal{I}_j \leq 2$  (i.e., both indicator functions can be 1). In contrast, if  $\mathcal{A}_{(i,j)} = 1$ , then  $\mathcal{I}_i + \mathcal{I}_j \leq 1$  (i.e., at most one of the two indicators can be 1). In our considered UAV-based surveillance systems, it can be assumed that the UAVs are vertices and the edges can be established among the vertices (i.e., the UAVs) when the UAVs observe wider overlapping areas because monitoring an area with multiple UAVs is inefficient.

The optimization problem (8)–(11) for solving MWIS is a well-known NP-hard problem. To solve this MWIS problem in a computationally efficient manner, we resort to a message-passing approach, which is a message inferential method performed on the conflict graph. Algorithm 1 presents the entire procedure for solving the MWIS problem with message-passing. Note that the message-passing (also called belief propagation, in the literature) can be used to solve our given MWIS problem for any graph [67]. In the standard form, such an algorithm is required to iterate for a while before it converges to (or, stops and estimates) a solution, as illustrated in Algorithm 1. In every single iteration, each node in the graph sends the message to its adjacent neighbors. Each node compares its own weight with the summation of weights in adjacent neighbor nodes during the update phase (line 6–11). Subsequently, each node computes its beliefs and determines whether it should be scheduled or not during the estimation phase (line 12–19). If the number of iterations increases, the comparison propagates, i.e., observing more information in the graph is possible.

---

**Algorithm 1** Message-passing for MWIS-based energy-efficient surveillance scheduling

---

- 1: Input:  $\mathcal{A}_{(i,j)}$  by (6), and  $w_i$  by (12), where  $s_i \in \mathcal{S}, s_j \in \mathcal{S}$
  - 2: Output:  $\mathcal{I}_i$
  - 3:  $t \leftarrow 0, w_i \leftarrow Q_i(0)$  for all  $s_i \in \mathcal{S}$
  - 4: **while** Each unit time  $t \in \{0, 1, \dots, T - 1\}$  **do**  $\triangleright T$  is the maximum number of time iteration.
  - 5:   Initialize  $m_{i \rightarrow j}^1(t) = 0$  and  $m_{j \rightarrow i}^1(t) = 0$  for all  $s_i \in \mathcal{S}, s_j \in \mathcal{S}$
  - 6:   **► Update Phase**
  - 7:   **while** Each iteration time  $n \in \{2, 3, \dots, K\}$  **do**  $\triangleright K$  is the number of message-passing iteration.
  - 8:     Calculate the message  $m_{i \rightarrow j}^{n+1}(t) \leftarrow \max\{0, w_i - \sum_{k \in \{\mathcal{N}(i)-j\}} m_{i \rightarrow k}^n(t)\}, \forall s_j \in \mathcal{N}(i)$ .
  - 9:     UAV  $s_i$  sends  $m_{i \rightarrow j}^{n+1}(t)$  to all  $s_j \in \mathcal{N}(i)$ .
  - 10:     Update  $n \leftarrow n + 1$ .
  - 11:   **end while**
  - 12:   **► Estimation Phase**
  - 13:   Calculate the belief  $b_{i \rightarrow j}^K(t) \leftarrow \sum_{s_k \in \mathcal{N}(i)} m_{k \rightarrow j}^K, \forall s_j \in \mathcal{N}(i)$ .  $\triangleright$  Belief is the lastly received message.
  - 14:   **if**  $b_{i \rightarrow j}^K(t) < w_i$  **then**
  - 15:      $\mathcal{I}_i = 1$ , where  $s_i \in \mathcal{S}$ , then  $s_i \in \mathcal{S}^*$   $\triangleright$  UAV  $s_i$  is scheduled (i.e., its camera is turned on).
  - 16:   **else**
  - 17:      $\mathcal{I}_i = 0$ , where  $s_i \in \mathcal{S}$ , then  $s_i \in \mathcal{U}$   $\triangleright$  UAV  $s_i$  is not scheduled (i.e., its camera is turned off).
  - 18:   **end if**
  - 19:   Update  $t \leftarrow t + 1$ .
  - 20: **end while**
-

We use the Jaccard similarity index [68], one of the standard measures used to calculate the similarity between two data points, in order to numerically determine the overlapping areas. The Jaccard similarity index is the ratio of cardinality of co-rated items to that of all items rated by both UAVs; thus, it can be calculated, as follows:

$$Sim(i, j) \triangleq \frac{|a_i \cap a_j|}{|a_i \cup a_j|} = \frac{|a_i \cap a_j|}{|a_i| + |a_j| - |a_i \cap a_j|}, \tag{13}$$

where  $a_i$  and  $a_j$  are the monitoring areas that contain spots by  $s_i$  and  $s_j$ , respectively. If the Jaccard similarity index is high among two adjacent UAVs, the UAVs observe overlapping areas, spatially and temporally at the same time. Therefore, the edge can be set to 1 in our considered conflict graph when the UAVs are assumed to be vertices in the conflict graph.

#### 4.2.2. Joint Optimization for Charging Matching and Wireless Energy Transfer

The unscheduled UAVs turn off their built-in cameras because they do not need to monitor the corresponding target areas and require recharging their batteries, as described in Section 4.2.1. Suppose that the set of unscheduled UAVs requires charging from the set of charging towers as depicted in Figure 1. As illustrated in Figure 1, the charging towers are connected to a single controller, which is a charging tower center that makes decisions for the joint optimization for charging matching (i.e., decisions for charging matching of UAVs and charging towers in terms of maximizing charging amounts) and wireless energy transfer (i.e., decisions for the amounts of wirelessly transferred energy for the matched UAVs and their associated charging towers), in each unit period  $t$ .

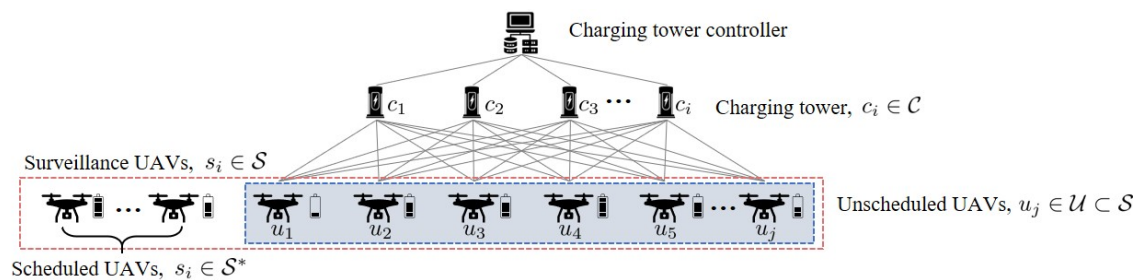


**Figure 1.** System model for the unscheduled unmanned aerial vehicles (UAVs) in terms of charging tower scheduling and wireless energy transfer decisions.

Let  $c_i$  and  $u_j$  denote charging towers and unscheduled UAVs, where  $\forall i \in \{1, \dots, |\mathcal{C}|\}$  and  $\forall j \in \{1, \dots, |\mathcal{U}|\}$ , respectively. We assume that each charging tower can charge multiple unscheduled UAVs simultaneously. The set of unscheduled UAVs (i.e.,  $\mathcal{U}$ ) is determined as the set of  $u_j$ , where  $u_j \in \{s_j \mid \mathcal{I}_j = 0, \text{ where } s_j \in \mathcal{S}\}$ . Therefore, the set of unscheduled UAVs is the subset of total UAVs  $\mathcal{S}$ , denoted as  $\mathcal{U} \subseteq \mathcal{S}$ . We assume that every unscheduled UAV is associated with only one charging tower. In this joint optimization problem for charging matching and wireless energy transfer, the objective is

to maximize the total amount of charging energy from the charging towers during time  $t$ . Our given problem can be formulated, as follows:

$$\max : \sum_{\forall c_i \in \mathcal{C}}, \sum_{\forall u_j \in \mathcal{U}} e_{(i,j)}(t) \cdot x_{(i,j)}(t), \tag{14}$$

$$\text{s.t.} \quad \sum_{\forall u_j \in \mathcal{U}} e_{(i,j)}(t) \cdot x_{(i,j)}(t) \leq C_i^{\max}(t), \forall c_i \in \mathcal{C}, \tag{15}$$

$$\sum_{\forall u_j \in \mathcal{U}} x_{(i,j)}(t) \leq n_i, \forall c_i \in \mathcal{C}, \tag{16}$$

$$\sum_{\forall c_i \in \mathcal{C}} x_{(i,j)}(t) \leq 1, \forall u_j \in \mathcal{U}, \tag{17}$$

$$e_{(i,j)}(t) \leq \min \left\{ E_j^{\max} - e_j(t + \Delta t_{(j \rightarrow i)}), \delta_j - E_j^{tr}(\Delta t_{tr}) \right\}, \forall c_i \in \mathcal{C}, \forall u_j \in \mathcal{U}, \tag{18}$$

$$e_{(i,j)}(t) \geq 0, \forall c_i \in \mathcal{C}, \forall u_j \in \mathcal{U}, \tag{19}$$

$$x_{(i,j)}(t) \in \{0, 1\}, \forall c_i \in \mathcal{C}, \forall u_j \in \mathcal{U}. \tag{20}$$

In this mathematical program (14)–(20), if the charging matching of charging tower  $c_i$  to UAV  $u_j$  is established,  $x_{(i,j)}(t) = 1$ , otherwise  $x_{(i,j)}(t) = 0$  according to (20). In addition, the amounts of charged energy from  $c_i$  to  $u_j$  are denoted as  $e_{(i,j)}(t)$ , according to (19). As indicated in (18), the amount of charging from charging tower  $c_i$  to its associated UAV  $u_j$  during the period  $t$  should consider the travel time of the UAVs to reach their associated towers. In (18),  $e_j(t + \Delta t_{(j \rightarrow i)})$  stands for the current energy status of UAV  $u_j$  at time  $t + \Delta t_{(j \rightarrow i)}$ , where  $\Delta t_{(j \rightarrow i)}$  represents the travel time, while UAV  $u_j$  moves to its associated charging tower  $c_i$ . The  $\delta_j$  indicates the amount of charging of  $u_j$  within  $t$ , and  $E_j^{tr}(\Delta t_{tr})$  stands for the expenditure of energy during the round-trip travel time  $\Delta t_{tr}$  (i.e., the UAV  $u_j$  travels to its associated charging tower  $c_i$  and returns to its original position or flies to a new waypoint), as described in (4). Subsequently, charging tower  $c_i$  can charge the battery for the UAV  $u_j$  by as much as  $\min \{ E_j^{\max} - e_j(t + \Delta t_{(j \rightarrow i)}), \delta_j - E_j^{tr}(\Delta t_{tr}) \}$ , as formulated in (18). Moreover, each UAV  $u_j$  can be associated with one charging tower  $c_i$ , as formulated in (17). Moreover, each charging tower  $c_i$  can have  $n_i$  multiple charging panels [69]; thus, they can be associated with multiple UAVs, as many as  $n_i$ , as shown in (16). Each charging tower  $c_i$  has its own energy budget (i.e., capacity)  $C_i^{\max}(t)$ , as shown in (15). Finally, conducting the joint optimization to maximize the total energy transfer from the charging towers to their associated UAVs is performed by computing the variables  $x_{(i,j)}(t)$  and  $e_{(i,j)}(t)$ , as shown in (14).

**Theorem 1.** *The program in (14)–(20) is non-convex.*

**Proof.** Here, we have to prove that (14) and (15) are not convex in this mathematical program (14)–(20). Note that the proof considers the simplest case at first (i.e.,  $|\mathcal{C}| = |\mathcal{U}| = 1$ ). In this case, (14) becomes  $a_{(i,j)}(t) \cdot x_{(i,j)}(t)$ . Let this equation be denoted by  $f$ . To show that this given equation is non-convex, the eigenvalues of the second-order Hessian of this given real function should be nonpositive definite [70]. The Hessian  $\nabla^2 f$  is as follows, where the two variables in (14) are  $e_{(i,j)}(t)$  and  $x_{(i,j)}(t)$ :  $\begin{bmatrix} 0 & 1 \\ 1 & 0 \end{bmatrix}$  and then the corresponding two eigenvalues are  $\pm 1$ . Not all of these values are nonnegative, which indicates that the Hessian is not positive definite, thus finally proving that the optimization function is non-convex. For (15), in a similar way, the corresponding two eigenvalues of the given second-order Hessian matrix are  $\pm 1$ ; thus, not all of the values are nonnegative (i.e., it also proves that the optimization function is non-convex). Finally, (14) and (15) are not non-convex. Thus, the program (14)–(20) is not convex.  $\square$

Because the optimal solutions cannot be obtained in non-convex programming, this non-convex programming must be converted to convex programming, if possible.

**Theorem 2.** *The use of*

$$e_{(i,j)}(t) \leq \min \left\{ E_j^{\max} - e_j(t + \Delta t_{(j \rightarrow i)}), \delta_j - E_j^{tr}(\Delta t_{tr}) \right\} \cdot x_{(i,j)}(t), \forall c_i \in \mathcal{C}, \forall u_j \in \mathcal{U}, \quad (21)$$

instead of (18) converts the given non-convex optimization program (14)–(20) into a convex one.

**Proof.** For the non-convex program (14)–(20),  $x_{(i,j)}(t) = 0$  indicates that the charging matching between  $u_j$  and  $c_i$  does not happen. Thus, the corresponding wireless energy transfer does not exist (i.e.,  $e_{(i,j)}(t) = 0$ ), and (21) leads to the same result when  $x_{(i,j)}(t) = 0$ :

$$e_{(i,j)}(t) \leq \min \left\{ E_j^{\max} - e_j(t + \Delta t_{(j \rightarrow i)}), \delta_j - E_j^{tr}(\Delta t_{tr}) \right\} \cdot \underbrace{0}_{x_{(i,j)}(t)=0} = 0, \forall c_i \in \mathcal{C}, \forall u_j \in \mathcal{U}, \quad (22)$$

However, (21) is equivalent to (18) when  $x_{(i,j)}(t) = 1$ . Therefore, we can replace  $e_{(i,j)}(t) \cdot x_{(i,j)}(t)$  with  $e_{(i,j)}(t)$ . Thus, (14) can also be updated, as follows:

$$\max : \sum_{\forall c_i \in \mathcal{C}} \sum_{\forall u_j \in \mathcal{U}} e_{(i,j)}(t), \quad (23)$$

and then, (15) is also updated, as follows:

$$\sum_{\forall u_j \in \mathcal{U}} e_{(i,j)}(t) \leq C_i^{\max}(t), \forall c_i \in \mathcal{C}, \quad (24)$$

Subsequently, no non-convex terms do not exist in this proposed program (14)–(20), which means that we can obtain optimal solutions for this mathematical program in polynomial time.  $\square$

Eventually, the final form of the joint optimization of charging matching and wireless energy transfer in each unit period  $t$  can be expressed, as follows:

$$\max : \sum_{\forall c_i \in \mathcal{C}}, \sum_{\forall u_j \in \mathcal{U}} e_{(i,j)}(t), \quad (25)$$

$$\text{s.t.} \quad \sum_{\forall u_j \in \mathcal{U}} e_{(i,j)}(t) \leq C_i^{\max}(t), \forall c_i \in \mathcal{C}, \quad (26)$$

$$\sum_{\forall u_j \in \mathcal{U}} x_{(i,j)}(t) \leq n_i, \forall c_i \in \mathcal{C}, \quad (27)$$

$$\sum_{\forall c_i \in \mathcal{C}} x_{(i,j)}(t) \leq 1, \forall u_j \in \mathcal{U}, \quad (28)$$

$$e_{(i,j)}(t) \leq \min \left\{ E_j^{\max} - e_j(t + \Delta t_{(j \rightarrow i)}), \delta_j - E_j^{tr}(\Delta t_{tr}) \right\} \cdot x_{(i,j)}(t), \forall c_i \in \mathcal{C}, \forall u_j \in \mathcal{U}, \quad (29)$$

$$e_{(i,j)}(t) \geq 0, \forall c_i \in \mathcal{C}, \forall u_j \in \mathcal{U}, \quad (30)$$

$$x_{(i,j)}(t) \in \{0, 1\}, \forall c_i \in \mathcal{C}, \forall u_j \in \mathcal{U}. \quad (31)$$

The equations (i.e., (25)–(31)) in this mathematical program are all linear combinations by Theorems 1 and 2. The program determines the charging matching of  $u_j$  to  $c_i$  and the charging energy transfer from  $c_i$  to its associated  $u_j$  in each  $t$ . At the end of each period, the remaining energy of each UAV can be calculated, as follows: XXX

$$e_j(t+1) \triangleq \begin{cases} e_j(t) - E_j^{hc}(t), & \text{UAV } u_j \text{ for task (i): hovering for surveillance,} \\ e_j(t) + e_{(i,j)}(t) - E_j^{tr}(\Delta t_{tr}), & \text{UAV } u_j \text{ for task (ii): round-trip traveling to charging tower,} \end{cases} \quad (32)$$

where the energy of hovering and communications (i.e.,  $E_j^{hc}(t)$  in (2)) is considered on top of current energy status  $e_j(t)$ , in the case of task (i). For the case of task (ii), the energy of traveling (i.e.,  $E_j^{tr}(\Delta t_{tr})$  in (4)) is expended and, moreover, the amount of charging energy (i.e.,  $e_{(i,j)}(t)$ , which is the optimal solution of mathematical program (25)–(31)) is recharged.

For this convex programming problem (25)–(31), we use an off-the-shelf software package, called CVX and MOSEK, for solving the mixed-integer convex optimization problem [71,72]. Consequently, we propose a polynomial-time optimization framework for the joint optimization of the charging matching of UAVs to charging towers and the wireless energy transfer between UAVs and charging towers, as shown in our final mathematical program (25)–(31).

#### 4.3. Computational Complexity

The computational complexity of the proposed algorithm can be separately discussed in the two separable problems, i.e., (i) MWIS-based UAV scheduling via message-passing and (ii) joint charging matching and wireless energy transfer. The first problem is originally NP-hard, because it is pure MWIS. Message-passing is used, which works in polynomial-time, in order to relax the NP-hard computational complexity. In addition, the second problem is originally formulated in the form of non-convex, however, the problem is converted into convex based on Theorems 1 and 2. Therefore, this problem also works in polynomial-time. Finally our proposed framework works in polynomial-time because two separable and sequential problems are all with polynomial-time operations.

### 5. Performance Evaluation

The performance of our proposed energy-efficient UAV-based surveillance system is simulated and evaluated in this section. This section presents the basic simulation setup (refer to Section 5.1) and it discusses the simulation results (refer to Section 5.2).

#### 5.1. Simulation Setup

*Surveillance UAVs.* We consider a DJI Phantom4 Pro v2.0 drone (DJI, Shenzhen, China) equipped with a surveillance camera [73]. The built-in battery in the drone permits a maximum flight time of 30 min in windless conditions. The altitude of the UAVs is set to 100 m; thus, the shapes and areas of corresponding surveillance areas are identical. The initial energies of the UAV batteries are uniform-randomly selected within [4000, 5870] mAh with the output voltage of 17.4 V.

*Monitoring Map.* We consider a well-known  $3 \times 3$  Manhattan grid map [74]. As shown in Figure 2, we place four charging towers at the apexes of a virtual rectangle. We assume that each charging tower has four charging panels. In the middle of the map, one ground station controls the flight of the UAVs and has enough charging panels to charge all given UAVs. In order to easily calculate the overlapping areas of UAVs, we define the grid-shaped 1479 reference points every 25 m in the Manhattan map as shown in Figure 2. Therefore, we regard the overlapping area in this paper as the number of reference points between UAVs by calculating Jaccard similarity index of (13) by counting the numbers, spatially and temporally at the same.

*Deployment Scenarios.* For the simulation study, we consider both fixed UAVs (F-UAVs) and moving UAVs (M-UAVs) that fly waypoints every unit period. We assume three different types of deployments for the F-UAVs as follows.

1. Scenario 1 (sparse lattice grid): 28 F-UAVs monitor the entire map without overlapping areas.
2. Scenario 2 (dense lattice grid): 45 F-UAVs monitor the entire map with overlapping areas that are fully covered without any blank space.
3. Scenario 3 (random): 20 F-UAVs are uniform-randomly distributed within the map.

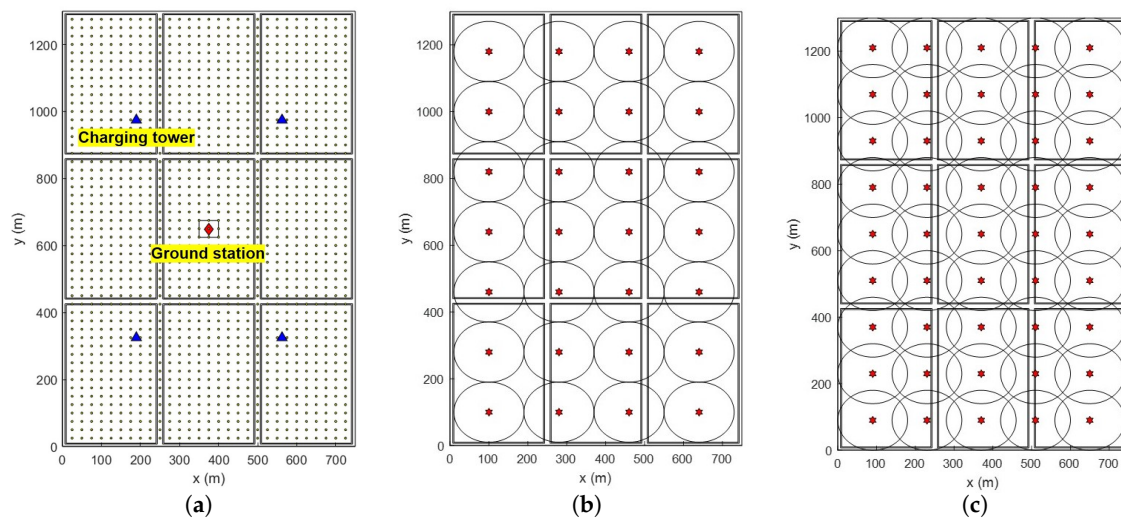


**Figure 2.** (a)  $3 \times 3$  Manhattan grid map with four charging towers and one ground station, and 1479 reference points of 25 m intervals (b) Scenario 1 (sparse lattice grid): 28 fixed UAVs without overlapping areas (c) Scenario 2 (dense lattice grid): 45 fixed UAVs with overlapping areas.

Scenarios 1 and 2 are both illustrated in Figure 2. Moreover, 10 M-UAVs fly along certain trajectories that consist of the sequences of waypoints. For realistic trajectories, we adopt the scan, oval, stay-at, eight, and waypoint movement based on the Paparazzi mobility model [75], as listed in Table 2. In each scenario, 5 or 10 M-UAVs are deployed. With the given topology, we simulate the surveillance systems for one or two hours while assuming each unit period repeats every 10 minutes. Note that the environmental setup parameters are summarized in Table 3.

**Table 2.** Trajectory of moving unmanned aerial vehicles (M-UAVs) every 10 minutes.

	Movement	10 min	20 min	30 min	40 min	50 min	60 min
M-UAV 1	Scan	(125, 1075)	(625, 1075)	(625, 650)	(125, 650)	(125, 225)	(625, 225)
M-UAV 2	Oval	(375, 1175)	(200, 1075)	(125, 900)	(125, 650)	(125, 400)	(200, 225)
M-UAV 3	Stay-at	(275, 800)	(175, 625)	(275, 425)	(475, 425)	(575, 625)	(475, 800)
M-UAV 4	Eight	(625, 475)	(575, 250)	(375, 150)	(175, 250)	(150, 475)	(375, 650)
M-UAV 5	Waypoint	(100, 100)	(150, 200)	(200, 300)	(250, 400)	(300, 500)	(350, 600)
M-UAV 6	Scan	(625, 225)	(125, 225)	(125, 650)	(625, 650)	(625, 1075)	(125, 1075)
M-UAV 7	Oval	(550, 1075)	(625, 900)	(625, 650)	(625, 400)	(550, 225)	(375, 150)
M-UAV 8	Stay-at	(475, 800)	(575, 625)	(475, 425)	(275, 425)	(175, 625)	(275, 800)
M-UAV 9	Eight	(150, 825)	(175, 1025)	(375, 1100)	(575, 1025)	(625, 825)	(375, 650)
M-UAV 10	Waypoint	(650, 1200)	(600, 1100)	(550, 1000)	(500, 900)	(450, 800)	(400, 700)
	Movement	70 min	80 min	90 min	100 min	110 min	120 min
M-UAV 1	Scan	(125, 225)	(125, 650)	(625, 650)	(625, 1075)	(125, 1075)	(625, 1075)
M-UAV 2	Oval	(375, 150)	(550, 225)	(625, 400)	(625, 650)	(625, 900)	(550, 1075)
M-UAV 3	Stay-at	(275, 800)	(175, 625)	(275, 425)	(475, 425)	(575, 625)	(475, 800)
M-UAV 4	Eight	(625, 825)	(575, 1025)	(375, 1100)	(175, 1025)	(150, 825)	(625, 475)
M-UAV 5	Waypoint	(400, 700)	(450, 800)	(500, 900)	(550, 1000)	(600, 1100)	(650, 1200)
M-UAV 6	Scan	(625, 1075)	(625, 650)	(125, 650)	(125, 225)	(625, 225)	(125, 225)
M-UAV 7	Oval	(200, 225)	(125, 400)	(125, 650)	(125, 900)	(200, 1075)	(375, 1175)
M-UAV 8	Stay-at	(475, 800)	(575, 625)	(475, 425)	(275, 425)	(175, 625)	(275, 800)
M-UAV 9	Eight	(150, 475)	(175, 250)	(375, 150)	(575, 250)	(625, 475)	(625, 475)
M-UAV 10	Waypoint	(350, 600)	(300, 500)	(250, 400)	(200, 300)	(150, 200)	(100, 100)

*Baseline of Comparison.* To demonstrate the effectiveness of our proposed algorithm, the performance is evaluated and compared to the performance of the battery-based algorithm as the baseline, which is the most straightforward and advanced method [76,77]. The operation of the battery-based algorithm is as follows:

- First, all of the UAVs perform their own major tasks (i.e., monitoring at their locations to the extent of their batteries). The charging tower controller checks the status of each battery of the UAVs and suspends the surveillance functionality if the battery remains below 30%.
- Next, the UAVs with battery status values of less than 30% select the nearest charging tower from their locations if the charging tower has available charging panels.

**Table 3.** Environmental setup parameters.

UAV Parameters	Value
Aircraft size (L × W × H)	289.5 mm × 289.5 mm × 196 mm
Aircraft weight	1375 g
Flight speed (max)	20 m/s
Field of view	84 degree
Flight time (max)	30 min
Capacity of flight battery	5870 mAh
Charging power of flight battery (max)	160 W
Voltage of charger	17.4 V
Rated power of charger	100 W
Charging efficiency loss	1.1
System Parameters	Value
Size of Manhattan map	1299 m × 750 m
Number of reference points	1479
Number of UAVs in Scenario 1	F-UAVs: 28, M-UAVs: 5 and 10
Number of UAVs in Scenario 2	F-UAVs: 45, M-UAVs: 5 and 10
Number of UAVs in Scenario 3	F-UAVs: 20, M-UAVs: 10
Altitude of surveillance UAVs	100 m
Number of charging towers	4
Number of charging panels in the charging tower	4
Number of charging panels in the ground station	50
Simulation time	60 and 120 min

## 5.2. Evaluation Results

Figure 3 presents the ratio of the UAV-covered area (i.e., surveillance enabled area), which is compared to the ratio of the total area of the Manhattan map. The cumulative saved energy denotes the hovering and communication-related energy for unscheduled UAVs. The connectivity of the conflict graphs updates according to the overlapping threshold setting, associated with the number of reference points in overlapping areas, calculated by Jaccard similarity index (JSI) in this paper, as presented in (13). The lower JSI increases the number of edges in the corresponding conflict graph. Subsequently, relatively small numbers of UAVs are scheduled. On the other hand, a high JSI decreases the number of edges in the given corresponding conflict graph. Therefore, a relatively substantial number of UAVs can be scheduled to suspend surveillance, which can reduce the overall hovering energy consumption. Consequently, we consider various JSI settings to numerically estimate the corresponding effects. Our proposed algorithm is named EE, which stands for energy-efficient UAV scheduling as compared to the baseline algorithm is noted as BB for battery-based algorithm.

In Figure 3, the ratio of the covered area decreases in Scenarios 1 and 2. This is because the residual batteries of UAVs become low, resulting in numerous UAVs needing to be charged as time goes by. Nevertheless, the EE algorithm reduces the performance degradation of the monitoring area through the efforts of the MWIS-based UAV scheduling compared to the BB algorithm. In Scenario 1, the deployment scenario has few overlapping areas, and each UAV plays a key role due to sparse deployment. Thus, the results reveal that it has more drawbacks in Scenario 1 in terms of coverage performance than the performance in Scenario 2. To compare the two algorithms, the EE algorithm tends to gradually decrease the surveillance area, whereas the BB algorithm sharply decreases the surveillance area in Scenarios 1 and 2. The cumulative saved energy is related to the number of unscheduled UAVs. The proposed EE algorithm with JSI = 0.5 is superior to the BB algorithm in the view of energy savings for the first 40 min. In addition to this energy efficiency, it also has better performance in terms of surveillance coverage ratios. In the last 10 min., the BB algorithm has a poorly

covered area of less than half of the total area; thus, the results of energy efficiency are meaningless. Lastly, in each scenario, 10 M-UAVs improve the coverage and energy performance in comparison with five UAVs. A larger number of UAVs create more edges in the given corresponding conflict graph; thus, our EE algorithm provides better performance in every case.

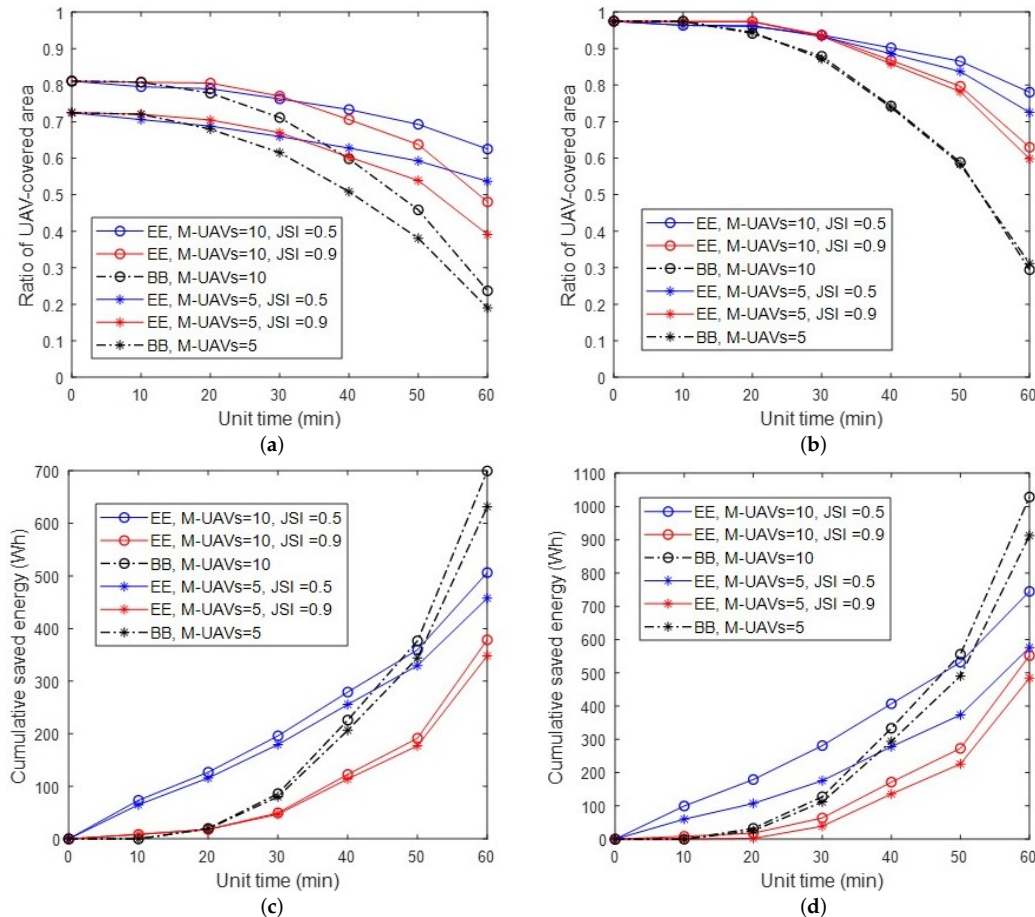


**Figure 3.** Ratio of UAV-covered surveillance area and cumulative saved energy of unscheduled UAVs for the proposed EE algorithm ( $JSI = 0.5$  and  $JSI = 0.9$ ), and BB algorithm where moving UAV (M-UAV) = 5 and moving UAV (M-UAV) = 10 (Scenario 1: 28 fixed UAVs (F-UAVs) and Scenario 2: 45 fixed UAVs (F-UAVs)). (a) Ratio of UAV-covered area (Scenario 1). (b) Ratio of UAV-covered area (Scenario 2). (c) Cumulative saved energy (Scenario 1). (d) Cumulative saved energy (Scenario 2).

Figure 4 and Table 4 display the number of unscheduled UAVs and their standard deviations  $\sigma$ , a statistic that measures the dispersion of a dataset relative to its mean and is calculated as the square root of the variance, in Scenario 3. In the early part of the simulation results, with  $JSI = 0.75$  (higher JSI), fewer UAVs are unscheduled (in other words, most of the UAVs are scheduled), owing to the few edges in its corresponding conflict graph. In contrast, for the simulation results with  $JSI = 0.125$  (a smaller JSI), its associated conflict graph is densely connected. Therefore, more UAVs are unscheduled when compared to the case of a higher JSI. The number of unscheduled UAVs increases in the later part of the simulation due to battery limitations. To maintain the number of scheduled UAVs as uniformly as possible during the simulation, the results with lower JSI present better performance than those with a higher JSI. A smaller standard deviation in Table 4 means the number of unscheduled UAVs (i.e., the UAVs with deactivated CCTV cameras) that are not changing dramatically. Therefore, the number of scheduled UAVs becomes stable; eventually reducing the chances of surveillance performance degradation. Moreover, the stable results show that the proposed algorithm is superior in

terms of energy-efficiency that is beneficial for extending surveillance lifetime and maximizing the charging energy.

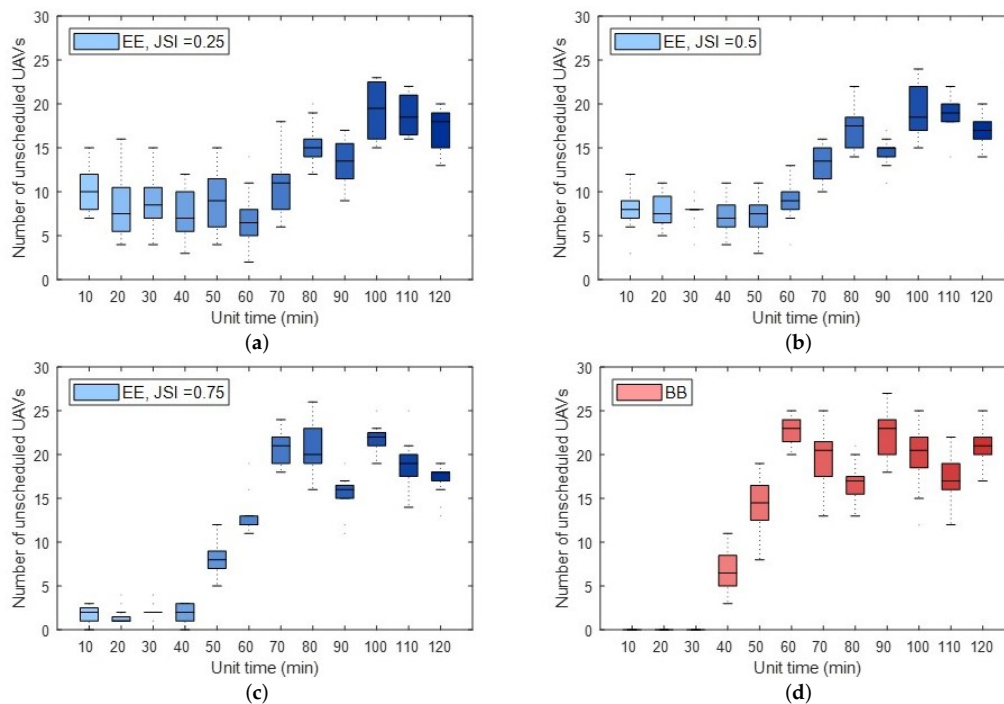


**Figure 4.** (a) EE algorithm, JSI = 0.25. (b) EE algorithm, JSI = 0.5. (c) EE algorithm, JSI = 0.75. (d) BB algorithm. The number of unscheduled UAVs for the proposed EE algorithm (JSI = 0.25, JSI = 0.5, and JSI = 0.75), and BB algorithm (Scenario 3: 20 F-UAVs, 10 M-UAVs).

**Table 4.** Standard deviation ( $\sigma$ ) of the number of unscheduled UAVs for both proposed algorithms, EE and BB (Scenario 3: 20 fixed UAVs (F-UAVs), 10 moving UAVs (M-UAVs)).

	Proposed EE Algorithm								BB Algorithm
JSI	0.125	0.25	0.375	0.5	0.625	0.75	0.875	1.0	
$\sigma$	4.564	4.900	5.001	5.798	6.783	8.054	8.814	9.387	9.162

Figure 5 presents the trade-off between the ratio of UAV-covered surveillance area and the amount of saved energy of the EE algorithm in Scenario 3. The ratio of the UAV-covered area is compared to the ratio of the area at the initial states, where all of the UAVs are scheduled. In the corresponding setting, the minimum and maximum JSI are 0.125 and 1, respectively. Here, the appropriate JSI setting plays a key role in achieving better performance. In order to guarantee a wider surveillance area coverage, a higher JSI is used to put more weight on the ratio of the UAV-covered surveillance area and a lower weight on the queue stability (i.e., related to energy status). In contrast, the lower JSI leads to the reduction of the ratio of the UAV-covered surveillance areas, whereas it is beneficial in efficient aspects. The optimal JSI value depends on the real-world system parameter configurations (e.g., the number of charging towers, the number of UAVs, and the amount of energy that can be charged in each charging panel) and quality-of-service (QoS) requirements (e.g., target monitoring area and target saving energy).

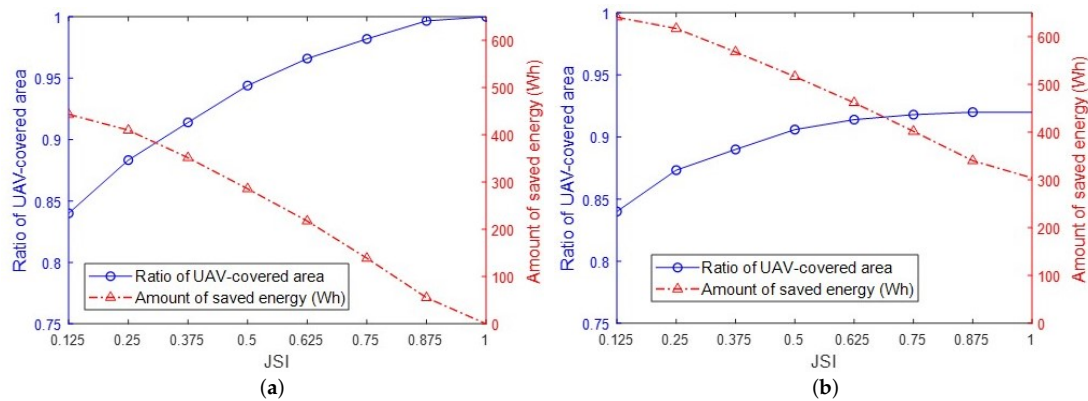


**Figure 5.** Trade-off between the ratio of the UAV-covered surveillance area and the amount of saved energy of the proposed EE algorithm (Scenario 3). (a) For 40 min. (b) For 60 min.

## 6. Concluding Remarks

This paper is the first attempt to design a legitimate UAV-based surveillance system where a charging infrastructure exists. We propose an energy-efficient UAV-based surveillance system that operates from two different perspectives (i.e., micro in-device operation and macro systemwide operation). The main objective of the micro in-device operation is to pursue energy-efficient operations by deactivating the CCTV cameras of the set of UAVs located in overlapping surveillance areas. For scheduling (i.e., obtaining the set of UAVs that are with activated CCTV surveillance cameras), a message-passing based algorithm is used because the overlapping situations are formulated with MWIS where the weight factors are defined as the residual battery values of individual UAVs because the message-passing is a well-known solution approach for MWIS formulation. The unscheduled UAVs (i.e., the UAVs that have deactivated CCTV cameras) fly to the charging towers to be charged. For the consequential macro system-wide operation, we aim at the computation for the optimal matching of UAVs to charging towers with a maximum amount of energy allocation. This joint optimization program for scheduling and energy allocation was initially formulated as non-convex, and then reformulated to convex, which can guarantee optimal solutions in polynomial time. Our proposed framework achieves the desired performance improvement in terms of energy consumption of unscheduled UAVs, the energy efficiency of each charging UAV, and efficient surveillance, as presented in the performance evaluation. Our proposed model can also be applied to drone taxi services. As future research directions, dynamic and adaptive control for JSI can be carefully considered because it is one of key factors that can lead to performance improvements in real-world implementation.

**Author Contributions:** S.J., J.-H.K., and J.K. were the main researchers who initiated and organized the research reported in this paper, and all authors were responsible for analyzing the simulation results and writing the paper. All authors have read and agreed to the published version of the manuscript.

**Funding:** This research was supported by the MSIT (Ministry of Science and ICT), Korea, under the ITRC (Information Technology Research Center) support program (IITP-2020-2017-0-01637) supervised by the IITP (Institute for Information & Communications Technology Promotion).

**Acknowledgments:** J.-H.K. is the corresponding author of this paper.

**Conflicts of Interest:** The authors declare no conflict of interest.

## References

- Shen, Y.; Pan, Z.; Liu, N.; You, X. Joint Design and Performance Analysis of a Full-Duplex UAV Legitimate Surveillance System. *Electronics* **2020**, *9*, 407. [\[CrossRef\]](#)
- Abdallah, A.; Ali, M.Z.; Mišić, J.; Mišić, V.B. Efficient Security Scheme for Disaster Surveillance UAV Communication Networks. *Information* **2019**, *10*, 43. [\[CrossRef\]](#)
- Kim, J.; Caire, G.; Molisch, A.F. Quality-Aware Streaming and Scheduling for Device-to-Device Video Delivery. *IEEE/ACM Trans. Netw.* **2016**, *24*, 2319–2331. [\[CrossRef\]](#)

4. Lee, H.; Lee, K.-J.; Kim, H.; Lee, I. Wireless Information and Power Exchange for Energy-Constrained Device-to-Device Communication. *IEEE Internet Things J.* **2018**, *5*, 3175–3185. [[CrossRef](#)]
5. Asiedu, D.K.P.; Lee, H.; Lee, K.-J. Simultaneous Wireless Information and Power Transfer for Decode-and-Forward Multihop Relay Systems in Energy-Constrained IoT Networks. *IEEE Internet Things J.* **2019**, *6*, 9413–9426. [[CrossRef](#)]
6. Na, W.; Park, J.; Lee, C.; Park, K.; Kim, J.; Cho, S. Energy-Efficient Mobile Charging for Wireless Power Transfer in Internet of Things Networks. *IEEE Internet Things J.* **2018**, *5*, 79–92. [[CrossRef](#)]
7. Lee, H.; Lee, S.-R.; Lee, K.-J.; Kong, H.-B.; Lee, I. Optimal Beamforming Designs for Wireless Information and Power Transfer in MISO Interference Channels. *IEEE Trans. Wirel. Commun.* **2015**, *14*, 4810–4821. [[CrossRef](#)]
8. Park, L.; Jeong, S.; Lakew, D.S.; Kim, J.; Cho, S. New Challenges of Wireless Power Transfer and Secured Billing for Internet of Electric Vehicles. *IEEE Commun. Mag.* **2019**, *57*, 118–1241. [[CrossRef](#)]
9. Al-Khafajiy, M.; Baker, T.; Hussien, A.; Cotgrave, A. UAV and Fog Computing for IoE-Based Systems: A Case Study on Environment Disasters Prediction and Recovery Plans. In *Unmanned Aerial Vehicles in Smart Cities*; Springer: Cham, Switzerland, 2020; Volume 1, pp. 133–152.
10. Mozaffari, M.; Saad, W.; Bennis, M.; Nam, Y.-H.; Debbah, M. A Tutorial on UAVs for Wireless Networks: Applications, Challenges, and Open Problems. *IEEE Commun. Surv. Tutor.* **2019**, *21*, 2334–2360. [[CrossRef](#)]
11. Mozaffari, M.; Kasgari, A.T.Z.; Saad, W.; Bennis, M.; Debbah, M. Beyond 5G With UAVs: Foundations of a 3D Wireless Cellular Network. *IEEE Trans. Wirel. Commun.* **2019**, *18*, 357–372. [[CrossRef](#)]
12. Mozaffari, M.; Saad, W.; Bennis, M.; Debbah, M. Communications and Control for Wireless Drone-Based Antenna Array. *IEEE Trans. Commun.* **2019**, *67*, 820–834. [[CrossRef](#)]
13. Khuwaja, A. A.; Chen, Y.; Zhao, N.; Alouini, M.; Dobbins, P. A Survey of Channel Modeling for UAV Communications. *IEEE Commun. Surv. Tutor.* **2018**, *20*, 2804–2821. [[CrossRef](#)]
14. Khawaja, W.; Guvenc, I.; Matolak, D.W.; Fiebig, U.; Schneckenburger, N. A Survey of Air-to-Ground Propagation Channel Modeling for Unmanned Aerial Vehicles. *IEEE Commun. Surv. Tutor.* **2019**, *21*, 2361–2391. [[CrossRef](#)]
15. Ma, Z.; Ai, B.; He, R.; Wang, G.; Niu, Y.; Zhong, Z. A Wideband Non-Stationary Air-to-Air Channel Model for UAV Communications. *IEEE Trans. Veh. Technol.* **2020**, *69*, 12140–1226. [[CrossRef](#)]
16. Cheng, X.; Li, Y. A 3-D Geometry-Based Stochastic Model for UAV-MIMO Wideband Nonstationary Channels. *IEEE Internet Things J.* **2019**, *6*, 1654–1662. [[CrossRef](#)]
17. Han, S.; Choi, J.; Kim, J. Numerical Approximation of Millimeter-Wave Frequency Sharing between Cellular Systems and Fixed Service Systems. *J. Commun. Netw.* **2020**, *22*, 37–45. [[CrossRef](#)]
18. Kim, J.; Lee, W. Feasibility Study of 60 GHz Millimeter-Wave Technologies for Hyperconnected Fog Computing Applications. *IEEE Internet Things J.* **2017**, *4*, 1165–1173. [[CrossRef](#)]
19. Kim, J.; Kwon, S.; Choi, G. Performance of Video Streaming in Infrastructure-to-Vehicle Telematic Platforms With 60-GHz Radiation and IEEE 802.11ad Baseband. *IEEE Trans. Veh. Technol.* **2016**, *65*, 10111–10115. [[CrossRef](#)]
20. Kim, J.; Molisch, A.F. Fast Millimeter-Wave Beam Training with Receive Beamforming. *J. Commun. Netw.* **2014**, *16*, 512–522. [[CrossRef](#)]
21. Dabiri, M.T.; Safi, H.; Parsaefard, S.; Saad, W. Analytical Channel Models for Millimeter Wave UAV Networks Under Hovering Fluctuations. *IEEE Trans. Wirel. Commun.* **2020**, *19*, 2868–2883. [[CrossRef](#)]
22. Najafi, M.; Ajam, H.; Jamali, V.; Diamantoulakis, P.D.; Karagiannidis, G.K.; Schober, R. Statistical Modeling of the FSO Fronthaul Channel for UAV-Based Communications. *IEEE Trans. Commun.* **2020**, *68*, 3720–3736. [[CrossRef](#)]
23. Zhang, L.; Zhao, H.; Hou, S.; Zhao, Z.; Xu, H.; Wu, X.; Wu, Q.; Zhang, R. A Survey on 5G Millimeter Wave Communications for UAV-Assisted Wireless Networks. *IEEE Access* **2019**, *7*, 117460–117504. [[CrossRef](#)]
24. Zhang, S.; Zhang, H.; Di, B.; Song, L. Cellular UAV-to-X Communications: Design and Optimization for Multi-UAV Networks. *IEEE Trans. Wirel. Commun.* **2019**, *18*, 1346–1359. [[CrossRef](#)]
25. Zeng, Y.; Wu, Q.; Zhang, R. Accessing From the Sky: A Tutorial on UAV Communications for 5G and Beyond. *Proc. IEEE* **2019**, *107*, 2327–2375. [[CrossRef](#)]
26. Huang, H.; Huang, C.; Ma, D. A Method for Deploying the Minimal Number of UAV Base Stations in Cellular Networks. *IEEE/CAA J. Autom. Sin.* **2020**, *7*, 559–567. [[CrossRef](#)]

27. Xu, D.; Sun, Y.; Ng, D. W.K.; Schober, R. Multiuser MISO UAV Communications in Uncertain Environments With No-Fly Zones: Robust Trajectory and Resource Allocation Design. *IEEE Trans. Commun.* **2020**, *68*, 3153–3172. [[CrossRef](#)]
28. He, H.; Zhang, S.; Zeng, Y.; Zhang, R. Joint Altitude and Beamwidth Optimization for UAV-Enabled Multiuser Communications. *IEEE Commun. Lett.* **2017**, *22*, 344–347. [[CrossRef](#)]
29. Zhao, J.; Liu, J.; Jiang, J.; Gao, F. Efficient Deployment With Geometric Analysis for mmWave UAV Communications. *IEEE Wirel. Commun. Lett.* **2020**, *9*, 1115–1119. [[CrossRef](#)]
30. Li, M.; Hong, Y.; Zeng, C.; Song, Y.; Zhang, X. Investigation on the UAV-To-Satellite Optical Communication Systems. *IEEE J. Sel. Areas Commun.* **2018**, *36*, 2128–2138. [[CrossRef](#)]
31. Mozaffari, M.; Saad, W.; Bennis, M.; Debbah, M. Unmanned Aerial Vehicle With Underlaid Device-to-Device Communications: Performance and Tradeoffs. *IEEE Trans. Wirel. Commun.* **2016**, *15*, 3949–3963. [[CrossRef](#)]
32. Yang, Z.; Pan, C.; Pei, L.; Chen, M.; Shikh-Bahaei, M.; ElKashlan, M.; Nallanathan, A. Joint Power, Altitude, Location and Bandwidth Optimization for UAV With Underlaid D2D Communications. *IEEE Wirel. Commun. Lett.* **2019**, *8*, 524–527.
33. Liu, H.; Yoo, S.; Kwak, K.S. Opportunistic Relaying for Low-Altitude UAV Swarm Secure Communications with Multiple Eavesdroppers. *J. Commun. Netw.* **2018**, *20*, 496–508. [[CrossRef](#)]
34. Zhong, C.; Yao, J.; Xu, J. Secure UAV Communication With Cooperative Jamming and Trajectory Control. *IEEE Commun. Lett.* **2019**, *23*, 286–289. [[CrossRef](#)]
35. Wu, H.; Wei, Z.; Hou, Y.; Zhang, N.; Tao, X. Cell-Edge User Offloading via Flying UAV in Non-Uniform Heterogeneous Cellular Networks. *IEEE Trans. Wirel. Commun.* **2020**, *19*, 2411–2426. [[CrossRef](#)]
36. Baek, J.; Han, S. I.; Han, Y. Optimal UAV Route in Wireless Charging Sensor Networks. *IEEE Internet Things J.* **2020**, *7*, 1327–1335. [[CrossRef](#)]
37. Baek, J.; Han, S.I.; Han, Y. Energy-Efficient UAV Routing for Wireless Sensor Networks. *IEEE Trans. Veh. Technol.* **2020**, *69*, 1741–1750. [[CrossRef](#)]
38. Park, S.; Shin, C.S.; Jeong, D.; Lee, H. DroneNetX: Network Reconstruction Through Connectivity Probing and Relay Deployment by Multiple UAVs in Ad Hoc Networks. *IEEE Trans. Veh. Technol.* **2018**, *67*, 11192–11207. [[CrossRef](#)]
39. Baek, H.; Lim, J. Time Mirroring Based CSMA/CA for Improving Performance of UAV-Relay Network System. *IEEE Syst. J.* **2019**, *13*, 4478–4481. [[CrossRef](#)]
40. Wu, Q.; Zeng, Y.; Zhang, R. Joint Trajectory and Communication Design for Multi-UAV Enabled Wireless Networks. *IEEE Trans. Wirel. Commun.* **2018**, *17*, 2109–2121. [[CrossRef](#)]
41. Amer, R.; Saad, W.; Marchetti, N. Mobility in the Sky: Performance and Mobility Analysis for Cellular-Connected UAVs. *IEEE Trans. Commun.* **2020**, *68*, 3229–3246. [[CrossRef](#)]
42. Mu, C.; Zhang, Y. Learning-Based Robust Tracking Control of Quadrotor With Time-Varying and Coupling Uncertainties. *IEEE Trans. Neural Netw. Learn. Syst.* **2020**, *31*, 259–273. [[CrossRef](#)] [[PubMed](#)]
43. Lee, J.-H.; Park, K.-H.; Ko, Y.-C.; Alouini, M.-S. A UAV-Mounted Free Space Optical Communication: Trajectory Optimization for Flight Time. *IEEE Trans. Wirel. Commun.* **2020**, *19*, 1610–1621. [[CrossRef](#)]
44. Xu, J.; Zeng, Y.; Zhang, R. UAV-Enabled Wireless Power Transfer: Trajectory Design and Energy Optimization. *IEEE Trans. Wirel. Commun.* **2018**, *17*, 5092–5106. [[CrossRef](#)]
45. Zhang, G.; Wu, Q.; Cui, M.; Zhang, R. Securing UAV Communications via Joint Trajectory and Power Control. *IEEE Trans. Wirel. Commun.* **2019**, *18*, 1376–1389. [[CrossRef](#)]
46. Cui, M.; Zhang, G.; Wu, Q.; Ng, D.W.K. Robust Trajectory and Transmit Power Design for Secure UAV Communications. *IEEE Trans. Veh. Technol.* **2018**, *67*, 9042–9046. [[CrossRef](#)]
47. Motlagh, N.H.; Bagaa, M.; Taleb, T. Energy and Delay Aware Task Assignment Mechanism for UAV-Based IoT Platform. *IEEE Internet Things J.* **2019**, *6*, 6523–6536. [[CrossRef](#)]
48. Say, S.; Inata, H.; Liu, J.; Shimamoto, S. Priority-Based Data Gathering Framework in UAV-Assisted Wireless Sensor Networks. *IEEE Sens. J.* **2016**, *16*, 5785–5794. [[CrossRef](#)]
49. Zhan, C.; Zeng, Y.; Zhang, R. Energy-Efficient Data Collection in UAV Enabled Wireless Sensor Network. *IEEE Wirel. Commun. Lett.* **2018**, *7*, 328–331. [[CrossRef](#)]
50. Gong, J.; Chang, T.-H.; Shen, C.; Chen, X. Flight Time Minimization of UAV for Data Collection Over Wireless Sensor Networks. *IEEE J. Sel. Areas Commun.* **2018**, *36*, 1942–1954. [[CrossRef](#)]
51. Yang, D.; Wu, Q.; Zeng, Y.; Zhang, R. Energy Tradeoff in Ground-to-UAV Communication via Trajectory Design. *IEEE Trans. Veh. Technol.* **2018**, *67*, 6721–6726. [[CrossRef](#)]

52. Yang, Z.; Xu, W.; Shikh-Bahaei, M. Energy Efficient UAV Communication With Energy Harvesting. *IEEE Trans. Veh. Technol.* **2020**, *69*, 1913–1927. [[CrossRef](#)]
53. Bisio, I.; Garibotto, C.; Lavagetto, F.; Sciarrone, A.; Zappatore, S. Blind Detection: Advanced Techniques for WiFi-Based Drone Surveillance. *IEEE Trans. Veh. Technol.* **2019**, *68*, 938–946. [[CrossRef](#)]
54. Vahidi, V.; Saberinia, E.; Morris, B. T. OFDM Performance Assessment for Traffic Surveillance in Drone Small Cells. *IEEE Trans. Intell. Transp. Syst.* **2019**, *20*, 2869–2878. [[CrossRef](#)]
55. Hu, M.; Liu, W.; Peng, K.; Ma, X.; Cheng, W.; Liu, J.; Li, B. Joint Routing and Scheduling for Vehicle-Assisted Multidrone Surveillance. *IEEE Internet Things J.* **2019**, *6*, 1781–1790. [[CrossRef](#)]
56. Savkin, A. V.; Huang, H. A Method for Optimized Deployment of a Network of Surveillance Aerial Drones. *IEEE Syst. J.* **2019**, *13*, 4474–4477. [[CrossRef](#)]
57. Girma, A.; Bahadori, N.; Sarkar, M.; Tadewos, T.G.; Behnia, M.R.; Mahmoud, M. N.; Karimoddini, A.; Homaifar, A. IoT-enabled autonomous system collaboration for disaster-area management. *IEEE/CAA J. Autom. Sin.* **2020**, *7*, 1249–1262. [[CrossRef](#)]
58. Brik, B.; Ksentini, A.; Bouaziz, M. Federated Learning for UAVs-Enabled Wireless Networks: Use Cases, Challenges, and Open Problems. *IEEE Access* **2020**, *8*, 53841–53849. [[CrossRef](#)]
59. Sami Oubbati, O.; Atiquzzaman, M.; Ahamed Ahanger, T.; Ibrahim, A. Softwarization of UAV Networks: A Survey of Applications and Future Trends. *IEEE Access* **2020**, *8*, 98073–98125. [[CrossRef](#)]
60. Alsamhi, S.H.; Ma, O.; Ansari, M.S.; Almalki, F.A. Survey on Collaborative Smart Drones and Internet of Things for Improving Smartness of Smart Cities. *IEEE Access* **2019**, *7*, 128125–128152. [[CrossRef](#)]
61. Zhu, X.; Li, J.; Zhou, M.; Target Coverage-Oriented Deployment of Rechargeable Directional Sensor Networks With a Mobile Charger. *IEEE Internet Things J.* **2019**, *6*, 5196–5208. [[CrossRef](#)]
62. Zeng, Y.; Zhang, R. Energy-Efficient UAV Communication with Trajectory Optimization. *IEEE Trans. Wirel. Commun.* **2017**, *16*, 3747–3760. [[CrossRef](#)]
63. Filippone, A. *Flight Performance of Fixed and Rotary Wing Aircraft*; Elsevier: Amsterdam, The Netherlands, 2006.
64. Desset, C.; Debaillie, B.; Giannini, V.; Fehske, A.; Auer, G.; Holtkamp, H.; Wajda, W.; Sabella, D.; Richter, F.; Gonzalez, M.J.; et al. Flexible Power Modeling of LTE Base Stations. In Proceedings of the IEEE Wireless Communications and Networking Conference (WCNC), Paris, France, 1–4 April 2012.
65. Franco, C.D.; Buttazzo, G. Energy-Aware Coverage Path Planning of UAVs. In Proceedings of the IEEE International Conference on Autonomous Robot Systems and Competitions, Vila Real, Portugal, 8–10 April 2015.
66. Zeng, Y.; Xu, J.; Zhang, R. Energy Minimization for Wireless Communication With Rotary-Wing UAV. *IEEE Trans. Wirel. Commun.* **2019**, *18*, 2329–2345. [[CrossRef](#)]
67. Giaccone, P.; Shah, D. Message-passing for Wireless Scheduling: An Experimental Study. In Proceedings of the International Conference on Computer Communications and Networks (ICCCN), Zurich, Switzerland, 8–10 August 2010.
68. Tan, P.N.; Steinbach, M.; Karpatne, A.; Kumar, V. *Introduction to Data Mining*, 2nd ed.; Pearson: London, UK, 2019.
69. Shin, M.; Kim, J.; Levorato, M. Auction-Based Charging Scheduling With Deep Learning Framework for Multi-Drone Networks. *IEEE Trans. Veh. Technol.* **2019**, *68*, 4235–4248. [[CrossRef](#)]
70. Boyd, S.; Vandenberghe, L. *Convex optimization*; Cambridge University Press: Cambridge, UK, 2004.
71. Diamond, S.; Boyd, S. CVXPY: A Python-Embedded Modeling Language for Convex Optimization. *J. Mach. Learn. Res.* **2016**, *17*, 1–5.
72. Andersen, E.D.; Andersen, K.D. The MOSEK Interior Point Optimizer for Linear Programming: An Implementation of the Homogeneous Algorithm. *High Perform. Optim.* **2000**, *33*, 192–232.
73. DJI. *Phantom 4 Pro/Pro+ Series User Manual*; DJI: Shenzhen, China, 2020.
74. Technical Specification Group Radio Access Network; Study on LTE-Based V2X Services. 3GPP TR 36.885 V14.0.0. 2016. Available online: <https://www.3gpp.org/dynareport/36885.htm> (accessed on 1 July 2020).
75. Ons, B.; Alinoé, A.; Fabien, G.; Nicolas, L. A Mobility Model For UAV Ad hoc Network. In Proceedings of the International Conference on Unmanned Aircraft Systems, Orlando, FL, USA, 27–30 May 2014.

76. Lee, J.; Park, G.-L. Distance-Based Heuristic in Selecting a DC Charging Station for Electric Vehicles. In Proceedings of the International Workshop on Multi-disciplinary Trends in Artificial Intelligence, Bangalore, India, 8–10 December 2014.
77. Bi, R.; Xiao, J.; Pelzer, D.; Ciechanowicz, D.; Eckhoff, D.; Knoll, A. A simulation-based heuristic for city-scale electric vehicle charging station placement. In Proceedings of the International Conference on Intelligent Transportation Systems, Yokohama, Japan, 16–19 October 2017.



© 2020 by the authors. Licensee MDPI, Basel, Switzerland. This article is an open access article distributed under the terms and conditions of the Creative Commons Attribution (CC BY) license (<http://creativecommons.org/licenses/by/4.0/>).